

Optical manipulation of electronic dimensionality in a quantum material

Shaofeng Duan,^{1,*} Yun Cheng,^{2,*} Wei Xia,³ Yuanyuan Yang,¹ Fengfeng Qi,² Chaozhi Huang,¹ Tianwei Tang,¹ Yanfeng Guo,³ Dong Qian,¹ Dao Xiang,^{2,4,5,†} Jie Zhang,² and Wentao Zhang^{1,‡}

¹*Key Laboratory of Artificial Structures and Quantum Control (Ministry of Education), Shenyang National Laboratory for Materials Science, School of Physics and Astronomy, Shanghai Jiao Tong University, Shanghai 200240, China*

²*Key Laboratory for Laser Plasmas (Ministry of Education), School of Physics and Astronomy, Shanghai Jiao Tong University, Shanghai 200240, China*

³*School of Physical Science and Technology, ShanghaiTech University, Shanghai 201210, China*

⁴*Zhangjiang Institute for Advanced Study, Shanghai Jiao Tong University, Shanghai 200240, China*

⁵*Tsung-Dao Lee Institute, Shanghai Jiao Tong University, Shanghai 200240, China*

Abstract

Exotic phenomenon can be achieved in quantum materials by confining electronic states into two dimensions. For example, relativistic fermions are realised in a single layer of carbon atoms [1], the quantized Hall effect can result from two-dimensional (2D) systems [2, 3], and the superconducting transition temperature can be enhanced significantly in a one-atomic-layer material [4, 5]. Ordinarily, 2D electronic system can be obtained by exfoliating the layered materials, growing monolayer materials on substrates, or establishing interfaces between different materials. Herein, we use femtosecond infrared laser pulses to invert the periodic lattice distortion sectionally in a three-dimensional (3D) charge density wave material, creating macroscopic domain walls of transient 2D ordered electronic states with exotic properties. The corresponding ultrafast electronic and lattice dynamics are captured by time- and angle-resolved photoemission spectroscopy [6] and MeV ultrafast electron diffraction [7]. Surprisingly, a novel energy gap state, which might be a signature of light-induced superconductivity, is identified in the photoinduced 2D domain wall near the surface. Such optical modulation of atomic motion is a new path to realise 2D electronic states and will be a new platform for creating novel phases in quantum materials.

* These two authors contributed equally

† dxiang@sjtu.edu.cn

‡ wentaozhang@sjtu.edu.cn

The control of macroscopic quantum phenomena is the key to exploring quantum materials for applications. Ultrafast optical irradiation is a novel approach for manipulating quantum phases or even promoting the emergence of novel quantum phases, such as light-induced superconductivity [8, 9], optical switching to hidden phases [10, 11], coherent control of phases [12–15], ultrafast photon-induced metastable states [16, 17], and light-modulated exotic phases [18]. In particular, photons coherently coupled to the lattice vibrations or phase order parameter can largely drive the excitations far from equilibrium, which could be an effective method to realise novel phases in a material. However, the possibility of realising novel phases by optically manipulating electronic dimensionality is still a largely open subject.

Ultrafast photon excitation in a charge density wave (CDW) material can induce a complete inversion of the phase order via an electron–phonon scattering process, while the symmetry of the inverted phase ($\Phi = 1$) is equivalent to the original phase ($\Phi = -1$) [19]. Macroscopic domain walls, in which the electronic states are two dimensional (2D), possibly exist parallel to the surface at the interval between the inverted phase and the original phase (Fig. 1a). The distribution of the domain walls can be modelled by an equation of motion based on a spatially and temporally dependent double-wall Ginzburg–Landau potential [20, 21], and quasi-2D electronic states can be expected near the surface if the macroscopic domain wall is at or a few atomic layers below the surface. Photon-induced phase inversions were evident in SmTe_3 [22] from an ultrafast X-ray diffraction experiment and in TbTe_3 from an ultrafast optical experiment [20]. Such a phase inversion is also expected in the quasi-one-dimensional CDW material $\text{K}_{0.3}\text{MoO}_3$ based on ultrafast X-ray diffraction data [23]. However, such photon-induced 2D electronic states in the domain wall have never been identified in a material, and whether the states retain long-range order is still unclear experimentally.

Herein, we report the ultrafast photon-induced long-range 2D ordered electronic states at the surface in a three-dimensional (3D) CDW material. We used infrared ultrashort laser pulses to pump the sample and monitored the electronic structure and lattice dynamics by high-resolution time- and angle-resolved photoemission (trARPES) [6] and MeV ultrafast electron diffraction (UED) [7], respectively (Fig. 1b, see Methods). With improved energy and pump fluence resolution, the trARPES experiments showed evidence of 2D electronic states on the surface due to the ultrafast phase-inversion-induced macroscopic domain wall, which was confirmed by the temporal lattice distortion from high-resolution UED experiments and was consistent with the phenomenological theory based on a spatially and temporally dependent double-wall Ginzburg–

Landau potential. Interestingly, a gapped electronic state, which was possibly the signature of light-induced superconductivity, was discovered at the macroscopic domain wall.

The material we studied was 1T-TiSe₂, for which the CDW transition at 202 K (T_c) is possibly a result of the cooperation of the excitonic interactions and Jahn–Teller effect [21, 24–27]. Below T_c , the distortion of two adjacent Se-Ti-Se layers are anti-phase locked, forming a commensurate 3D CDW with a $2 \times 2 \times 2$ periodic lattice distortion (PLD) [28]. Our trARPES experiment at 4 K clearly showed a flattened “Mexican-hat” shaped dispersion in the Se $4p_{x,y}$ band, which is a signature of strong electron–hole interactions (left panel of Fig. 1c) [25, 29, 30]. We note that the 6.05-eV laser measured the band structures near the Γ point of the 3D Brillouin zone (Fig. 1b, see Methods) [30]. Equilibrium PLD was evident from the diffraction patterns (left panel of Fig. 1d). Furthermore, the Se $4p_{x,y}$ bands folded from point A ($A-4p_{x,y}$) and the Ti $3d_{z^2}$ band folded from point L ($L-3d_{z^2}$) due to the PLD were resolved. At 0.5 ps after the photoexcitation with a pump fluence higher than the breaking threshold of the excitonic correlation and CDW order [31–33], the flattened Se $4p_{x,y}$ band could not be well defined near the band top (central panel of Fig. 1c), which was possibly due to the strong CDW fluctuations. The PLD superlattice peaks were almost indistinguishable (right panel of Fig. 1d) at the same delay time, indicating that both the electronic order and the PLD could be completely suppressed at such a high pump fluence. Both the $L-3d_{z^2}$ band and the flattened Se $4p_{x,y}$ band were restored at a delay time of 12 ps (right panels of Fig. 1c), but with reduced binding energies compared to the equilibrium case. The superlattice diffraction signal was approximately half recovered, which is not shown here.

To track the ultrafast evolution of the CDW order, we will focus on the dynamics of the flattened Se $4p_{x,y}$ band at the Γ point. At an excitation fluence of 0.02 mJ/cm², the time-dependent photoemission spectrum and the PLD diffraction intensity clearly showed a band oscillation in both intensity and energy (Fig. 2), which was a result of photon-induced coherent A_{1g} -CDW phonons [32–35]. At the same high excitation fluence as that shown in Fig. 1c, the flattened $4p_{x,y}$ band was not resolvable until 1 ps after photon excitation due to strong electron–hole interactions (Fig. 2a). Two critical pump fluences with F_{c1} at 0.073 mJ/cm² (Fig. 2b) and F_{c2} at 0.135 mJ/cm² (Fig. 2c) were identified (Supplementary Information section II). As discussed in previous reports [32, 33], F_{c1} is the critical pump fluence for quenching the exciton condensation, and above F_{c2} , the PLD can be fully suppressed. In addition, intensity oscillations occur immediately after time zero at high pump fluence values, but detailed analysis showed that the oscillations were inharmonic, and the peak-to-peak distance was shorter than the period of the A_{1g} -CDW phonon oscillations

(Fig. 2c). Such an inharmonic oscillating state is a signature of a forced vibration, and the measured electronic states even temporally enter inverted CDW states, which is further confirmed by UED measurements. With increasing pump fluence, more time is required to reach a maximum suppression of the PLD peak, and the coherent oscillations even became invisible by increasing the pump fluence further (blue arrows in Fig. 2d), which is the signature of softening of the A_{1g} -CDW phonons. At the highest pump fluence, less time was required to reach the first maximum suppression of the CDW peak, and interestingly, a peak (red arrows in Fig. 2d) reappeared closer to time zero than the first oscillation peak at a low pump fluence, which was a result of pump-induced inhomogeneous PLD inversion in real space.

The above observations indicated the existence of photoinduced phase inversion in the TiSe_2 and was consistent with a simulation of the phase inversion scenario (see Methods and Supplementary Information section III). With such phase inversion, transient macroscopic domain walls parallel to the surface might be formed at long delay times following the phenomenological theory of a spatially and temporally dependent double wall Ginzburg–Landau potential [20, 21]. From the phenomenological theory, the distribution of the domain wall perpendicular to the sample surface can be tuned by the excitation pulse energy, and it can be expected that at certain pump fluences, transient macroscopic domain walls, which are possibly quasi-2D electronic systems, can be positioned near the sample surface (top panels in Fig. 3d).

TrARPES is an excellent tool for probing the transient electronic structure with surface sensitivity. The detailed pump-fluence-dependent photoemission spectra at the Γ point at a delay time of 12 ps showed that the photoemission intensity just slightly increased until a dramatic enhancement occurred above the fluence of about 0.070 mJ/cm^2 (Figs. 3a and d), close to the exciton condensation critical pump fluence F_{c1} . The upward shift at 0.070 mJ/cm^2 was a result of the pump-induced collapse of the CDW order that had not fully recovered at the delay time of 12 ps shown here. It is difficult to differentiate the energy of the $4p_{x,y}-3d_{z^2}$ flattened band from the A- $4p_{x,y}$ band precisely. However, since the A- $4p_{x,y}$ band was much weaker in intensity and closer to the Fermi energy than the $4p_{x,y}-3d_{z^2}$ band, we addressed the left edge shift (green cut in Fig. 3b) as a result of the shift of the $4p_{x,y}-3d_{z^2}$ band, which monotonically shifted upward with increasing pump fluence (Fig. 3c). Interestingly, the edge at the bottom right (red cut in Fig. 3b) of the $4p_{x,y}-3d_{z^2}$ band shifted upward dramatically at the pump fluence of $\sim 0.070 \text{ mJ/cm}^2$, reaching a maximum at $\sim 0.91 \text{ mJ/cm}^2$, and then dropped to a minimum at $\sim 0.116 \text{ mJ/cm}^2$. Upon enhancing the pump fluence further, the edge shifted to new maxima (at fluences of 0.156, 0.237, and

0.340 mJ/cm²) and then new minima (at fluences of 0.185, 0.273, and 0.371 mJ/cm²) alternately until reaching a point at which it monotonically increases at a high pump fluences. The edge at the upper right side (blue cut in Fig. 3b) of the $4p_{x,y}$ - $3d_{z^2}$ band was similar to that at the bottom right but with a weaker peak–dip feature, which was also attributed to the folded A- $4p_{x,y}$ band. Similar pump-induced downshifts also occurred in the intensity as a function of the pump fluence (Fig. 3d). The observed dips described above were results of the lower folding intensity from the A- $4p_{x,y}$ band, indicating that the electronic states at the dips with fluences of 0.116, 0.185, 0.273, and 0.371 mJ/cm² were possibly 2D. By solving the equation of motion based on the phenomenological Ginzburg–Landau potential (Supplementary Information section III), the 2D electronic structure was determined to be near the macroscopic domain wall where the Ginzburg–Landau potential ($V(\Phi)$) was a maximum (red curve in Fig. 3d). By comparing the experimental result to the solved equation of motion, the calculated $V(\Phi)$ must start near F_{c1} to match the experimental result, which means that the phase inversion was strongly correlated with the Jahn–Teller PLD and the order parameter in the Ginzburg–Landau potential does not need to include the contribution from the excitonic interactions necessarily.

In contrast, the intensity of the L - $3d_{z^2}$ band showed a minimum (maximum) at the same fluences where the $4p_{x,y}$ band edge reached a maximum (minimum) (Fig. 3d), indicating that the near Fermi energy density of states of the L - $3d_{z^2}$ band was enhanced in the photoinduced 2D electronic states (domain wall). Such photoinduced 2D electronic states, which result the peak-dip features in fluence dependent intensity of the $4p_{x,y}$ band, could also be identified at equilibrium temperatures of 30 and 80 K but were absent at 295 K (Fig. 4a), which is above the CDW transition temperature.

Recently, superconductivity was discovered in pressurised, Cu-intercalated, and electric-field controlled 1T-TiSe₂ [36–38]. The existence of an incommensurate CDW phase with localised commensurate CDW domains separated by domain walls is common in superconducting 1T-TiSe₂, and the enhancement of the density of states at the domain wall is believed to be responsible for the superconductivity. The 2D domain wall reported herein also showed an enhancement of the density of states near the Fermi energy (the intensity of the L - $3d_{z^2}$ band at 0.116 mJ/cm² in Fig. 3d). Such an enhancement of the density of states might also result in superconductivity in 1T-TiSe₂. A close comparison of the energy distribution curves (EDCs) for the pump fluences of 0.091 (peak) and 0.116 mJ/cm² (dip) at 4 K showed the signature of the opening of a small energy gap \sim 2 meV at the domain wall (Fig. 4c), although the electronic temperature was much higher than 4 K. An energy gap (\sim 1.5 meV) was also evident at the second domain wall on the

surface as the pump fluence was increased further (in the EDCs measured at 0.156 (peak) and 0.185 mJ/cm² (dip) in Fig. 4c), but no resolvable gap was found away from the domain wall. The energy gap here was obtained from the leading edge shift between the EDCs at the two pump fluences, which is a common method for determining the energy gap with a non-apparent coherent peak [39]). Energy gaps were also identified at 6 and 9 ps, which are not shown here. We note that in the superconducting Cu-intercalated 1T-TiSe₂, the estimated energy gap was about 0.5 meV [40], which was at the same scale as the domain-wall-induced energy gap, since the leading edge shift was just an estimate of the energy gap with an energy resolution of 19 meV. Interestingly, the electronic temperature estimated by fitting the Fermi edge to an energy-resolution-convolved Fermi–Dirac function was about 90 K, which is much higher than the equilibrium superconducting transition temperature in the pressurised, Cu-intercalated, and electric-field-controlled samples. In Fig. 4c, we compare EDCs between the peak and dip to extract the energy gap, because at these two corresponding excitation fluences, the electronic temperature was comparable and the temperature effect on the EDC could be excluded. We note that a leading edge shift did not appear in the inelastic scattered electrons, which represented the Fermi–Dirac broadening at these pump fluences (Fig. 4b).

The energy gap was still resolvable (~ 1 meV) at 30 K and was significantly smaller than that at 4 K, but it was difficult to determine at 80 K within the experimental resolution (Fig. 4c). A superconductor-like energy gap with a size comparable to the equilibrium superconducting gap was evident in K₃C₆₀ from the ultrafast optical spectra after pumping with an ultrashort far-infrared laser pulse at 100 K, which was significantly greater than its equilibrium superconducting transition temperature of 20 K [9]. The energy gap observed in the phase-inversion-induced domain wall was similar to the observation for K₃C₆₀, in which the energy gap was comparable to the equilibrium superconducting gap in spite of its much higher electronic temperature. Such a pump-induced energy gap at a high electronic temperature may share the same non-equilibrium physics, although they may have different mechanism origins. The pioneering observations of light-induced coherent conductivity at high temperatures in cuprates [8, 41], in which the studied materials also possessed high-temperature CDW phases, also possibly originated from the pump-induced macroscopic domain walls. Further experimental and theoretical work is required to clarify this.

In summary, we detected photo-induced macroscopic CDW domain walls in 1T-TiSe₂. The found domain walls existed parallel to the surface in the interval between the photo-inverted phase and the original phase and could be placed near the surface by finely tuning the excitation energy.

This macroscopic domain wall exhibited the behaviour of a 2D electronic system, and thus, it is a platform for realising novel phases, for example, phases with superconductivity. Our work presents a novel approach for manipulating quantum materials using ultrafast laser pumping, and open a new window in ultrafast science with profound implications for next-generation devices with new functionalities. However, further studies are necessary to clarify the precise mechanism for producing such macroscopic domain walls, to determine if such methods are universal and applicable for other CDW materials or even other ordered solids, and most interestingly, to identify if the observed energy gap was a result of photoinduced superconductivity.

I. METHODS

TrARPES. In the trARPES measurements, infrared photon pulses with wavelength centred at 700 nm (1.77 eV) and pulse length of 30 fs were used to excite the sample, and the non-equilibrium states were probed by ultraviolet pulses at 205 nm (6.05 eV). Both of the pump and probe beam are *s* polarized in our experimental geometry. The measurements were taken at $k_z = 2$ at the Fermi energy ($E_B = 0$) by $k_z = \frac{1}{\hbar} \sqrt{2m_e[(h\nu - W - |E_B|)\cos^2\theta + V_0]}$ with photon energy $h\nu = 6.05$ eV, system work function $W = 4.3$, nearly normal emission ($\theta = 0$), and inner potential $V_0 = 13.5$ eV in our experiments. The excitation fluences of the pump beam can be precisely tuned by using a half waveplate and a polarizer, and the size of pump pulse is 8.5 times larger than the probe beam, ensuring a fluence resolution of 2.5% in the fluence dependent measurements (Supplemental Information section IV). Photoelectrons were collected by a Scienta DA30L-8000R analyzer. The overall time resolution and energy resolution are 130 fs and 19 meV respectively [6]. Sample was cleaved at a pressure better than 3×10^{-11} torr at 4 K.

MeV UED. The structural dynamics was independently investigated by a MeV UED facility with a double bend achromat compressor. An 800 nm laser with about 30 fs pulse width was used to pump the sample and a 3 MeV electron beam is used to probe the dynamics. The electrons were produced in a photocathode radio-frequency gun and were further compressed to below 30 fs (FWHM) at the sample with the compressor [7]. The size of pump pulse is 5 times larger than the electron beam, thus ensuring uniform excitation on the sample. An electron-multiplying CCD camera and a phosphor screen are used to measure the diffraction pattern. High quality TiSe₂ thin film with a thickness of 60 nm was prepared by exfoliating a bulk single crystal. Sample was tilted by several degree to the normal incidence to avoid the intensity cancellation in the PLD diffraction

(Supplementary Information section I). During the experiment, the temperature of the sample was kept at ~ 90 K by liquid nitrogen.

Domain wall simulation. The pump-induced macroscopic domain wall can be modelled by solving a motion equation based on a spatially- and temporally-dependent double wall Ginzburg-Landau potential [20, 21]. The potential $V(\Phi, z)$, in which z is the depth away from the surface and Φ is the order parameter, is

$$V(\Phi, z) = \frac{1}{4}(\eta \cdot e^{-\frac{t}{\tau_e}} \cdot e^{-\frac{z}{z_p}} - 1)\Phi^2 + \frac{1}{8}\Phi^4 + \frac{1}{4}\xi^2\left(\frac{\partial\Phi}{\partial z}\right)^2. \quad (1)$$

Here $\eta e^{-\frac{t}{\tau_e}} e^{-\frac{z}{z_p}}$ is the transient change on the potential energy after photoexcitation with the pump fluence coefficient η , nonequilibrium quasiparticle recovery rate $\frac{1}{\tau_e} = 0.3 \text{ ps}^{-1}$ determined by experiment, and pump penetration depth $z_p = 17 \text{ nm}$ [42], and the CDW coherence length at low temperature $\xi = 1.2 \text{ nm}$ [20]. The third term results from inhomogeneous order parameter [43]. The temporally and spatially dependent order parameter $\Phi(z, t)$ can be numerically solved from the motion equation based on such a potential with the input of the above parameters in TiSe_2 (Fig. 3d). The procedure to do the solution is introduced in the Supplementary Information III.

II. ACKNOWLEDGMENTS

W.T.Z. acknowledges support from the Ministry of Science and Technology of China (2016YFA0300501) and from National Natural Science Foundation of China (11674224 and 11974243) and additional support from a Shanghai talent program. T.W.T. acknowledges support from National Natural Science Foundation of China (11704247). Y.F.G. acknowledges the support by the National Natural Science Foundation of China (Grant No. 11874264). D.Q. acknowledges support from the Ministry of Science and Technology of China (Grant No. 2016YFA0301003) and the National Natural Science Foundation of China (Grants No. U1632272 and No. 11521404). D.X. and J.Z. acknowledge support from the National Natural Science Foundation of China (Grants No. 11925505, 11504232, and 11721091) and from the office of Science and Technology, Shanghai Municipal Government (No. 16DZ2260200 and 18JC1410700).

III. AUTHOR CONTRIBUTIONS

S.F.D. and Y.C. contributed equally to this work. W.T.Z. and D.X. proposed and designed the research. S.F.D., Y.Y.Y., C.Z.H., T.W.T., and W.T.Z. contributed to the development and maintenance of the trARPES system. S.F.D., Y.Y.Y., and C.Z.H. collected the trARPES data. Y.C. and F.F.Q. took the UED measurements. W.X. and Y.F.G. prepared the single crystal sample. S.F.D., Y.C., D.X., and W.T.Z. did the phenomenological simulation. W.T.Z. wrote the paper with S.F.D., Y.C., D.Q., D.X., and J.Z. All authors discussed the results and commented on the manuscript.

IV. AUTHOR INFORMATION

Correspondence and requests for materials should be addressed to W.T.Z. (wentaozhang@sjtu.edu.cn; trARPES experimental data and the simulation) or D.X. (dxiang@sjtu.edu.cn; UED experimental data).

V. COMPETING INTERESTS

The authors declare that they have no competing financial interests.

-
- [1] Castro Neto, A. H., Guinea, F., Peres, N. M. R., Novoselov, K. S. & Geim, A. K. The electronic properties of graphene. *Reviews of Modern Physics* **81**, 109–162 (2009).
 - [2] von Klitzing, K., Dorda, G. & Pepper, M. New method for high-accuracy determination of the fine-structure constant based on quantized hall resistance. *Physical Review Letters* **45**, 494–7 (1980).
 - [3] Tsui, D. C., Stormer, H. L. & Gossard, A. C. Two-dimensional magnetotransport in the extreme quantum limit. *Physical Review Letters* **48**, 1559–62 (1982).
 - [4] He, S. L. *et al.* Phase diagram and electronic indication of high-temperature superconductivity at 65 k in single-layer FeSe films. *Nature Materials* **12**, 605–610 (2013).
 - [5] Tan, S. Y. *et al.* Interface-induced superconductivity and strain-dependent spin density waves in FeSe/SrTiO₃ thin films. *Nature Materials* **12**, 634–640 (2013).
 - [6] Yang, Y. *et al.* A time- and angle-resolved photoemission spectroscopy with probe photon energy up to 6.7 eV. *Review of Scientific Instruments* **90**, 063905 (2019).

- [7] Qi, F. F. *et al.* Breaking 50 femtosecond resolution barrier in mev ultrafast electron diffraction with a double bend achromat compressor. *Physical Review Letters* **124**, 134803 (2020).
- [8] Fausti, D. *et al.* Light-induced superconductivity in a stripe-ordered cuprate. *Science* **331**, 189–191 (2011).
- [9] Mitrano, M. *et al.* Possible light-induced superconductivity in K_3C_{60} at high temperature. *Nature* **530**, 461–464 (2016).
- [10] Ichikawa, H. *et al.* Transient photoinduced 'hidden' phase in a manganite. *Nature Materials* **10**, 101–105 (2011).
- [11] Stojchevska, L. *et al.* Ultrafast switching to a stable hidden quantum state in an electronic crystal. *Science* **344**, 177–180 (2014).
- [12] Rini, M. *et al.* Control of the electronic phase of a manganite by mode-selective vibrational excitation. *Nature* **449**, 72–74 (2007).
- [13] Li, X. *et al.* Terahertz field-induced ferroelectricity in quantum paraelectric $SrTiO_3$. *Science* **364**, 1079–1082 (2019).
- [14] Sie, E. J. *et al.* An ultrafast symmetry switch in a weyl semimetal. *Nature* **565**, 61–66 (2019).
- [15] Horstmann, J. G. *et al.* Coherent control of a surface structural phase transition. *Nature* **583**, 232–236 (2020).
- [16] Morrison, V. R. *et al.* A photoinduced metal-like phase of monoclinic VO_2 revealed by ultrafast electron diffraction. *Science* **346**, 445–448 (2014).
- [17] Nova, T. F., Disa, A. S., Fechner, M. & Cavalleri, A. Metastable ferroelectricity in optically strained $SrTiO_3$. *Science* **364**, 1075–1079 (2019).
- [18] Wang, Y. H., Steinberg, H., Jarillo-Herrero, P. & Gedik, N. Observation of floquet-bloch states on the surface of a topological insulator. *Science* **342**, 453–457 (2013).
- [19] Lian, C., Zhang, S.-J., Hu, S.-Q., Guan, M.-X. & Meng, S. Ultrafast charge ordering by self-amplified exciton-phonon dynamics in $TiSe_2$. *Nature Communications* **11**, 43 (2020).
- [20] Yusupov, R. *et al.* Coherent dynamics of macroscopic electronic order through a symmetry breaking transition. *Nature Physics* **6**, 681–684 (2010).
- [21] Schaefer, H., Kabanov, V. V. & Demsar, J. Collective modes in quasi-one-dimensional charge-density wave systems probed by femtosecond time-resolved optical studies. *Physical Review B* **89**, 045106 (2014).

- [22] Trigo, M. *et al.* Formation of buried domain walls in the ultrafast transition of SmTe_3 . *Arxiv:2006.08879* (2020).
- [23] Huber, T. *et al.* Coherent structural dynamics of a prototypical charge-density-wave-to-metal transition. *Physical Review Letters* **113**, 026401 (2014).
- [24] Di Salvo, F. J., Moncton, D. E. & Waszczak, J. V. Electronic properties and superlattice formation in the semimetal TiSe_2 . *Physical Review B (Solid State)* **14**, 4321–8 (1976).
- [25] Cercellier, H. *et al.* Evidence for an excitonic insulator phase in 1T- TiSe_2 . *Physical Review Letters* **99**, 146403 (2007).
- [26] Moehr-Vorobeva, E. *et al.* Nonthermal melting of a charge density wave in TiSe_2 . *Physical Review Letters* **107**, 036403 (2011).
- [27] Kogar, A. *et al.* Signatures of exciton condensation in a transition metal dichalcogenide. *Science* **358**, 1315–1317 (2017).
- [28] Hildebrand, B. *et al.* Local real-space view of the achiral 1T- TiSe_2 $2 \times 2 \times 2$ charge density wave. *Physical Review Letters* **120**, 136404 (2018).
- [29] Pillo, T. *et al.* Photoemission of bands above the fermi level: The excitonic insulator phase transition in 1T- TiSe_2 . *Physical Review B* **61**, 16213–16222 (2000).
- [30] Watson, M. D. *et al.* Orbital-and $k(z)$ -selective hybridization of Se 4p and Ti 3d states in the charge density wave phase of TiSe_2 . *Physical Review Letters* **122**, 076404 (2019).
- [31] Rohwer, T. *et al.* Collapse of long-range charge order tracked by time-resolved photoemission at high momenta. *Nature* **471**, 490–493 (2011).
- [32] Porer, M. *et al.* Non-thermal separation of electronic and structural orders in a persisting charge density wave. *Nature Materials* **13**, 857–861 (2014).
- [33] Hedayat, H. *et al.* Excitonic and lattice contributions to the charge density wave in 1T- TiSe_2 revealed by a phonon bottleneck. *Physical Review Research* **1**, 023029 (11 pp.) (2019).
- [34] Holy, J. A., Woo, K. C., Klein, M. V. & Brown, F. C. Raman and infrared studies of superlattice formation in TiSe_2 . *Physical Review B (Solid State)* **16**, 3628–37 (1977).
- [35] Snow, C. S., Karpus, J. F., Cooper, S. L., Kidd, T. E. & Chiang, T. C. Quantum melting of the charge-density-wave state in 1T- TiSe_2 . *Physical Review Letters* **91**, 136402 (2003).
- [36] Joe, Y. I. *et al.* Emergence of charge density wave domain walls above the superconducting dome in 1T- TiSe_2 . *Nature Physics* **10**, 421–425 (2014).

- [37] Yan, S. C. *et al.* Influence of domain walls in the incommensurate charge density wave state of Cu intercalated 1T-TiSe₂. *Physical Review Letters* **118**, 106405 (2017).
- [38] Li, L. J. *et al.* Controlling many-body states by the electric-field effect in a two-dimensional material. *Nature* **529**, 185–189 (2016).
- [39] Norman, M. R. *et al.* Destruction of the Fermi surface underdoped high-T_c superconductors. *Nature* **392**, 157–160 (1998).
- [40] Li, S. Y., Wu, G., Chen, X. H. & Taillefer, L. Single-gap s-wave superconductivity near the charge-density-wave quantum critical point in Cu_xTiSe₂. *Physical Review Letters* **99**, 107001 (2007).
- [41] Hu, W. *et al.* Optically enhanced coherent transport in YBa₂Cu₃O_{6.5} by ultrafast redistribution of interlayer coupling. *Nature Materials* **13**, 705–711 (2014).
- [42] Bayliss, S. C. & Liang, W. Y. Reflectivity, joint density of states and band structure of group IVb transition-metal dichalcogenides. *Journal of Physics C (Solid State Physics)* **18**, 3327–35 (1985).
- [43] McMillan, W. L. Landau theory of charge-density waves in transition-metal dichalcogenides. *Physical Review B* **12**, 1187–1196 (1975).

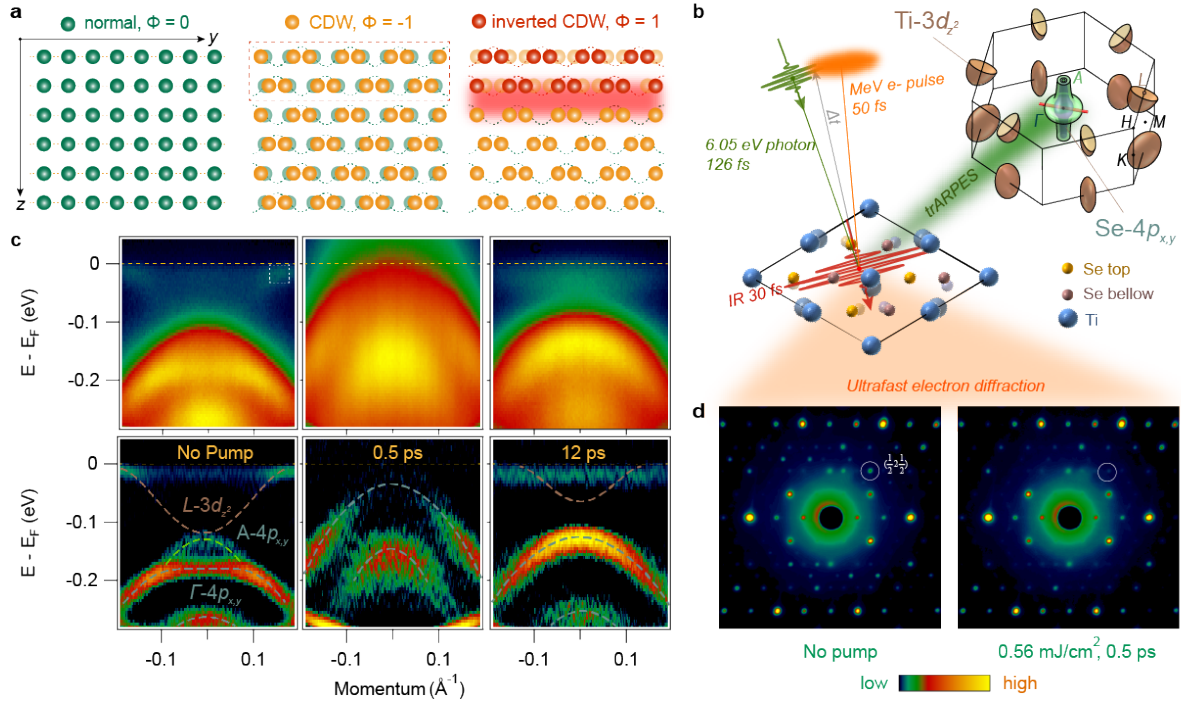


FIG. 1. Time-resolved electronic structure and electron diffraction patterns in TiSe₂. (a) Schematic of the charge density wave (CDW) inversion in real space (side view). The position of the top surface was defined as $z = 0$. The normal state lattice was $1 \times 1 \times 1$ with the order parameter $\Phi = 0$. The CDW lattice was $2 \times 2 \times 2$ with the order parameter $\Phi = -1$. The inverted layers were anti-phase distorted with the order parameter $\Phi = 1$. Upon photon excitation, phase inversion happens in the red dashed rectangle, and quasi 2D electronic states exist between the inverted and original CDW layers (red shaded area). (b) Experimental geometry of time- and angle-resolved photoemission (trARPES) and ultrafast electron diffraction (UED). Δt is the time delay between the infrared pump pulse and ultraviolet laser and MeV electron beams. The momentum cut (red line in the 3D Brillouin zone) in trARPES experiment is centered at Γ along $\Gamma - M$ direction. (c) Electronic structures with a pump fluence of 0.355 mJ/cm² and their corresponding 2nd derivative images along energy axis measured at 4 K. (d) Typical UED patterns of TiSe₂ before and after photoexcitation with a pump fluence of 0.56 mJ/cm² at 90 K. The white circle represents the $(\frac{1}{2}2\frac{1}{2})$ PLD peak.

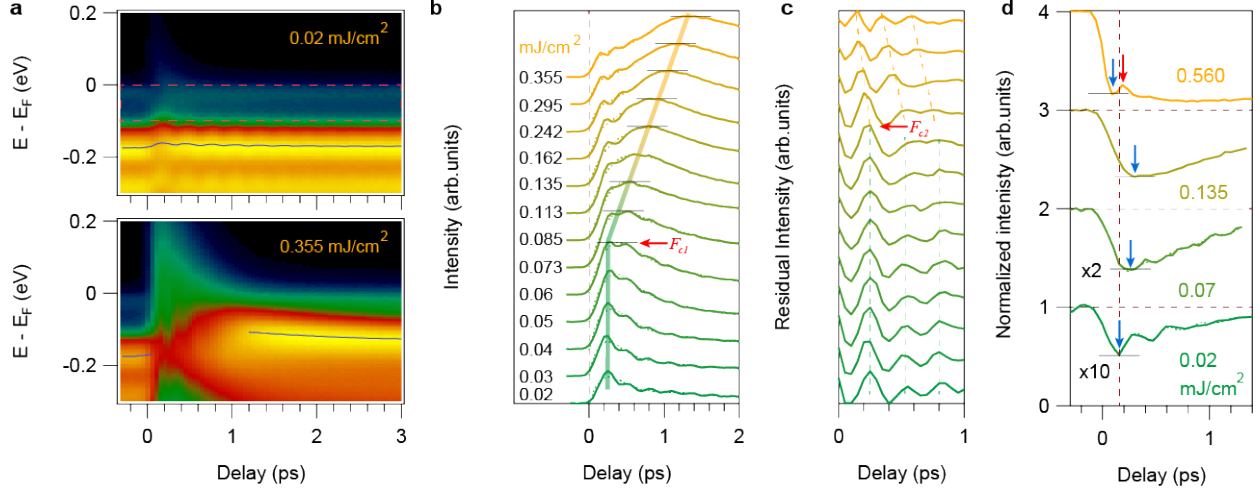


FIG. 2. Electronic structure and periodic lattice distortion (PLD) dynamics. (a) Time-dependent photoemission spectrum at Γ for low and high pump fluences. The blue curves are the position of the upper Se $4p_{x,y}$ band as a function of delay time by tracking the peak position at Γ . (b) Pump-fluence-dependent spectral intensity as a function of the delay time integrated from -0.1 eV (Se $4p_{x,y}$ band top) to the Fermi level highlighted by the red dashed box in panel (a). (c) Residual intensities after removing smooth backgrounds from the curves shown in (b). Red arrows denote the two critical pump fluences. (d) Pump-fluence-dependent diffraction intensity as a function of the delay time at the PLD peak ($\frac{1}{2}2\frac{1}{2}$). Blue arrows denote the delay time when the PLD intensity is mostly suppressed at corresponding pump fluences.

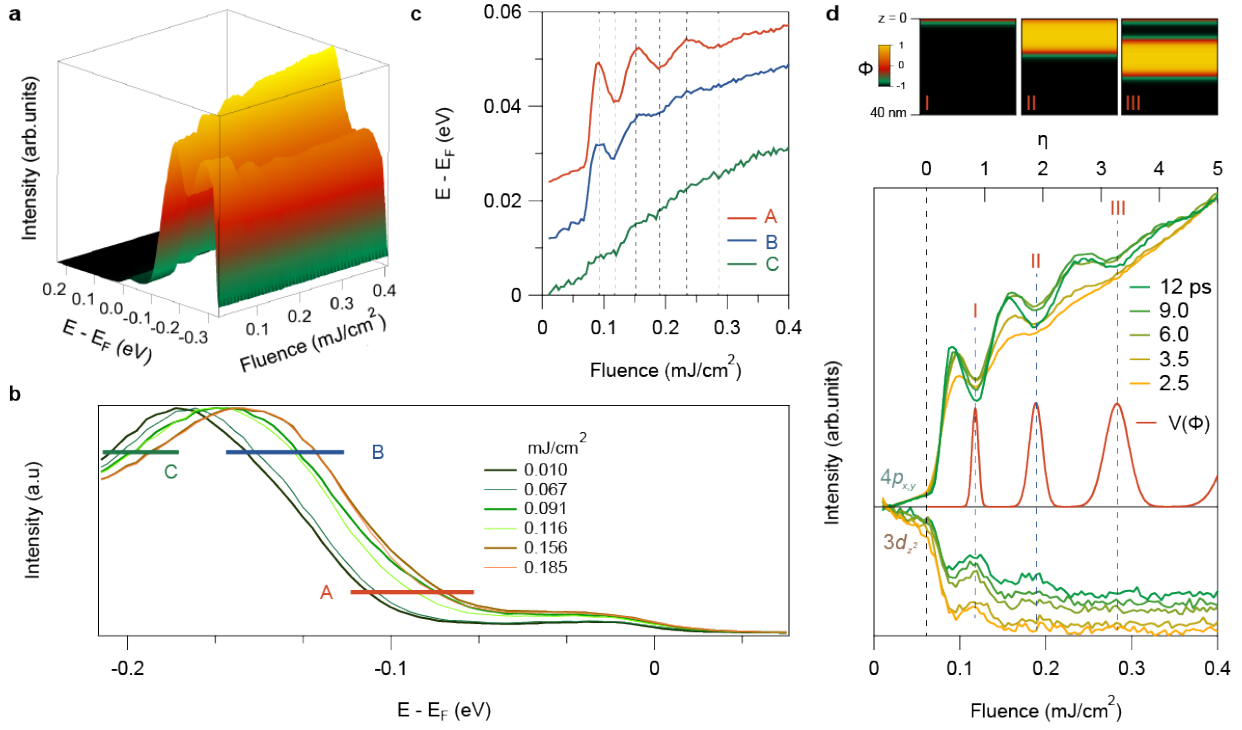


FIG. 3. Photoinduced domain wall. (a) Photoemission spectrum at Γ as a function of the pump fluence at 12 ps. (b) EDCs for pump fluences (0.01 and 0.067 mJ/cm^2) below F_{c1} and at the peaks (0.091 and 0.156 mJ/cm^2) and dips (0.116 and 0.185 mJ/cm^2) in (a) and (d). All the EDCs are normalized to the same height. (c) Fluence-dependent band edge shifts in energy at the cuts A, B, and C shown in (b). (d) Spectral intensity as a function of the pump fluence integrated from -0.1 eV (Se $4p_{x,y}$ band top) to the Fermi level and $L-3d_{z^2}$ band integrated in the dashed rectangle shown in the upper left panel of Fig. 1c. Calculated $V(\Phi)$ as a function of the pump fluence (η) at the surface ($z = 0$). All the curves are normalized to the same height. Calculated order parameters as a function of depth (z) for fluences at I, II, and III are plotted on the top of the panel.

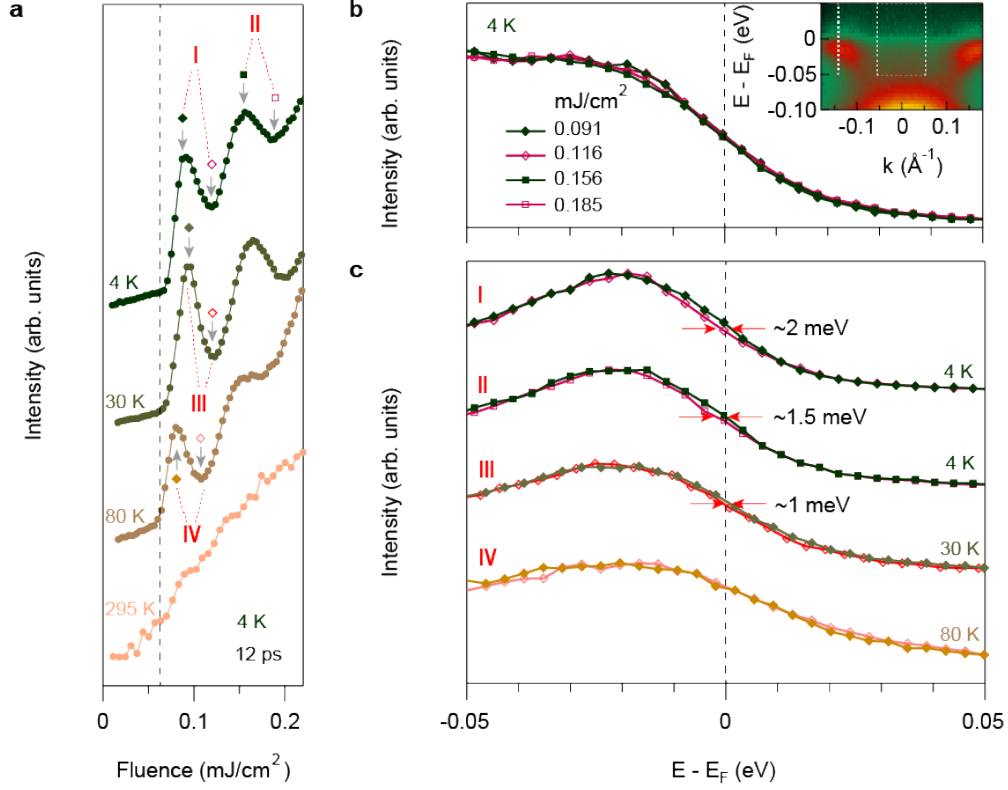


FIG. 4. Energy gap in the pump-induced domain wall. (a) Pump-induced photoemission intensity change between 0 and -0.1 eV at Γ as a function of the pump fluence at 4, 30, and 80 K and above the CDW transition temperature of 295 K. The measurements were taken 12 ps after the photoexcitation. (b) Integrated photoemission intensity as a function of energy between the momentum values of -0.05 and 0.05 \AA^{-1} (dashed rectangle in the inset) for pump fluences at the peaks and dips (domain walls) at 4 K shown in (a). (c) Energy distribution curves (EDCs) at the momentum of the dashed line shown in the inset of (b) for pump fluences at the peak-dip features (denoted by I, II, III, and IV in (a) and (c)). The red arrows show the energy gap open from the leading edge shift between pump fluences at the peaks and dips at 4 K and 30 K, but no signature of energy gap at 80 K within energy resolution. All the EDCs are normalized to the same height.